Pergamon

Acta mater. Vol. 45, No. 12, pp. 4953–4962, 1997

Printed in Great Britain
PII: S1359-6454(97)00197-3
1359-6454/97 $17.00 + 0.00

A FINITE ELEMENT METHOD FOR SIMULATING INTERFACE MOTION—II. LARGE SHAPE CHANGE DUE TO SURFACE DIFFUSION

B. SUN[1] and Z. SUO[2]*

[1]Applied Magnetics Corporation, 75 Robin Hill Road, Goleta, CA 93117, U.S.A. and [2]Mechanical and Aerospace Engineering Department, Princeton University, Princeton, NJ 08544, U.S.A.

(Received 24 January 1997; accepted 22 May 1997)

Abstract—This paper presents a finite element method for large shape change of a solid due to matter diffusion on its surface. The free energy, which motivates the change, is the surface energy summed over surface and grain boundary areas, Following a classical theory, we define the driving force by the amount of free energy decrease associated with per unit volume of matter moving per unit distance on the surface, and adopt a kinetic law that the matter flux on the surface is proportional to the driving force. We express this theory by a weak statement that forms the basis of the finite element method. In addition to surface diffusion, the weak statement includes evaporation and condensation, which allows a convenient treatment of mass conservation. We use these ideas to develop a general finite element program for two dimensional problems. The program is used to analyze thermal grooving on a polycrystalline surface, and the competition between surface grooving and grain boundary migration in a polycrystalline thin film. © *1997 Acta Metallurgica Inc.*

1. INTRODUCTION

Today finite element codes can analyze stress fields in complex materials and structures. No such codes exist, similarly accommodating and robust, to analyze evolving microstructures in materials. The object of this work is to develop finite element methods for motions of microscopic surfaces, driven by multiple energetic forces, via concomitant rate processes. In Part I of this work [1], we presented such a method for interface migration driven by interface tension and chemical energy difference between phases. We adopted a widely used kinetic law: the velocity of the interface is proportional to the driving pressure (i.e. the free energy reduction associated with the interface moving per unit distance). The computer program can simulate grain boundary migration, solid surface motion via evaporation–condensation, and their combination.

This paper extends Ref. [1] by including matter diffusion on the solid surface. Our method can be viewed as a numerical implementation of a classical theory discussed by Herring [2]. The theory assumes that the free energy of the system is the surface energy summed over all surface and grain boundary areas. To reduce this free energy, the solid changes shape by matter diffusion on the surface. This *global* energetic statement, however, is insufficient to determine the shape history, because infinitely many shape histories would each reduce the free energy. To complete the theory, Herring defined a driving force by the amount of free energy decrease associated with per unit volume of matter moving per unit distance on the surface. This definition prescribes a *local* quantity, the driving force, at every point on the solid surface. He then assumed a kinetic law that, at every point on the surface, the mass flux is proportional to the driving force. The formal procedure, incidentally, follows that of irreversible thermodynamics [3]. Other forms of energy (e.g. elastic energy, work done by an external force) can be readily added to the free energy.

The theory results in a partial differential equation with fourth-order differentials of surface geometry, and is non-linear when the shape change is large. Few analytic solutions exist. Mullins linearized the equation and analyzed grooving on a polycrystal surface [4], steady motion of a triple junction of the surface and a grain boundary [5], and flattening of a scratched surface [6]. Asaro and Tiller [7] discovered that a flat surface of a solid under an elastic strain is unstable and can undulate by surface diffusion; the instability may cause the surface to nucleate cracks [8], or break an epitaxial film into islands [9]. Chuang and Rice [10] gave a non-linear solution of a slit growing on a grain boundary, as matter diffuses from the slit surfaces into the grain boundary. Thouless [11] showed that surface diffusion

*To whom all correspondence should be addressed.

may limit the stress relaxation rate in a polycrystalline thin film.

Several phenomena have been analyzed with numerical methods, including grain boundary cavitation [12], powder sintering [13], crack nucleation on the surface of a stressed solid [14], and shape change of electromigration voids [15]. The methods are based on finite difference; they are conceptually simple and relatively fast. They require, however, very smooth representation of the surface because of the fourth-order differentials. They are inconvenient when other energetic forces and rate processes are present in a problem, or when the surface forms facets and corners due to, e.g. surface tension anisotropy or elastic field concentration.

To formulate numerical methods with low-order differentials, an established idea in continuum mechanics is to express a theory by an integral (or a weak) statement. Various forms of this idea include the Galerkin procedure, variational principles, and finite element methods [16]. In analyzing a void growing on a grain boundary, as matter diffuses on the grain boundary and creeps in the grains, Needleman and Rice [17] constructed a variational principle, which they used to formulate a finite element method. The variational principle found other applications [18, 19]. A similar variational principle was constructed to analyze large shape change due to surface diffusion [20, 21]; its applications were reviewed in [22]. Shape change of faceted surfaces was simulated with a related method [23].

In the previous papers [20–22], specific to each phenomenon, the solid shape was modeled with a few generalized coordinates; the Galerkin procedure reduced the weak statement to a set of ordinary differential equations that evolve the generalized coordinates. This paper describes a finite element method for general problems involving arbitrarily large shape change. The next section reviews Herring's theory, and formulates its weak statement. In contrast to evaporation–condensation treated in [1], surface diffusion requires that solid mass be conserved, making the above weak statement difficult to implement in a finite element setting. We then formulate a weak statement that circumvents the problem. This is followed by a section describing the finite element method. Numerical examples are given for thermal grooving on a polycrystal surface, and competitive motion of a grain boundary and a free surface in a polycrystalline thin film.

2. THEORY

2.1. Herring's theory

Herring's theory has three ingredients: energetics, kinetics, and kinematics [2]. As in [1], here we assume that the free energy consists of surface energy only, and that the surface tension γ, is isotropic (i.e. independent of crystalline direction). For a polycrystalline particle, γ can take different values on the surface and on the grain boundaries. The free energy of the particle is

$$G = \sum \gamma A. \tag{1}$$

The sum extends over all the surface and grain boundary areas, collectively denoted by A. As shown in [1], surface tension anisotropy presents no difficulty in the theory, but is ignored in this presentation for clarity. We also ignore the free energy associated with solid volume, such as that due to phase difference or elastic strain. Both could be readily added to the free energy. The addition of elastic energy, however, would require that an elastic field be determined for every solid shape during evolution.

Different from evaporation–condensation treated in [1], surface diffusion requires another set of kinetic and kinematic descriptions. To facilitate a comparison of the two processes, here we will formulate surface diffusion in a way that parallels evaporation –condensation in [1]. The solid changes its shape to reduce the free energy. This global statement can be used to prescribe a local quantity. Define the driving force, **F**, by the amount of free energy decrease associated with per unit volume of matter moving per unit distance on the surface. The driving force is a vector field tangent to the surface. Starting with this definition, Herring [2] related the driving force to the surface tension and the gradient of surface curvature. Our finite element method will use the basic definition, but not the explicit expression, of the driving force.

Figure 1 illustrates a portion of the surface in three dimensions. Denote the unit vector normal to a surface element by **n**. A contour lies on the surface, **m** being the unit vector lying in the surface, normal to a curve element. At a point on the contour, **m** and **n** are normal to each other, and both are normal to the tangent vector of the curve element. Let **J** be the flux, which is a vector field tangent to the surface, such that **J**·**m** is the volume of matter crossing per unit length of the curve per unit time.

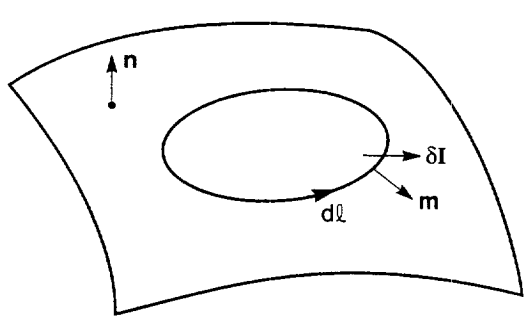

Fig. 1. A surface in three dimensions.

Following Herring, we adopt a kinetic law that, at every point on the surface, the flux is proportional to the driving force:

$$\mathbf{J} = \mathbf{M}\mathbf{F}. \tag{2}$$

Here $\mathbf{M}$ is the mobility of atoms on the surface. It is a second order tensor at any point on the surface, and may vary from point to point. In this work, the mobility is assumed to be isotropic, represented by a number related to the self-diffusivity by the Einstein relation, $\mathbf{M} = \Omega D\delta/kT$, where Ω is the volume per atom, D the self-diffusivity on the surface, δ the effective thickness of atoms participating in matter transport, k Boltzmann's constant, and T the absolute temperature.

In contrast to evaporation–condensation, surface diffusion leaves solid mass conserved. As matter diffuses on the surface, the solid recedes where matter depletes, and protrudes where matter accumulates. The change is purely kinematic. Let v_n be the normal velocity of the surface. Mass conservation requires that

$$v_n = -\nabla \cdot \mathbf{J}. \tag{3}$$

Here $\nabla\cdot\mathbf{J}$ stands for the surface divergence of the flux vector.

The above considerations are sufficient to compute the shape history. Given a solid shape, the curvature gradient causes the force $\mathbf{F}$, which, according to the kinetic law, drives the flux $\mathbf{J}$. To conserve solid mass, the divergence of the flux gives rise to the surface velocity, which then updates the shape for a small time increment. Repeat the procedure for many time increments to trace the evolving solid shape.

2.2. *Weak statement for surface diffusion*

We next express Herring's theory into a weak statement. A *virtual motion* of the surface slightly changes the solid shape, but conserves mass. The motion is otherwise unrestricted; in particular, it need not obey any kinetic law. Let $\delta\mathbf{I}$ be the mass displacement, which is a vector field tangent to the surface, such that $\delta\mathbf{I}\cdot\mathbf{m}$ is the volume of matter crossing per unit length of the curve on the surface. Let δr_n be the normal displacement of the surface (i.e. the volume of matter added to per unit area of the surface). By definition, $\delta\mathbf{I}$ and δr_n are the analogs of $\mathbf{J}$ and v_n, respectively, but have nothing to do with the time. Mass conservation demands a relation similar to (3):

$$\delta r_n = -\nabla \cdot (\delta\mathbf{I}). \tag{4}$$

Both $\delta\mathbf{I}$ and δr_n are fields that describe a virtual motion of the surface: they are small changes, and can take different magnitudes at different points on the surface, so long as they conserve mass according to (4).

We now express Herring's definition of the driving force into an integral form. Associated with any virtual motion of the surface, as specified by a pair of fields $\delta\mathbf{I}$ and δr_n subject to (4), the surface area changes, so does the free energy. Denote this free energy change by δG. Consider a differential element of the surface area, δA. Recall that the driving force, $\mathbf{F}$, is defined by the amount of free energy decrease associated with per unit volume of matter relocating per unit distance. Consequently, matter relocation on the area element $\mathrm{d}A$ reduces the free energy by $\mathbf{F}\cdot\delta\mathbf{I}\mathrm{d}A$. Thus,

$$\int \mathbf{F}\cdot\delta\mathbf{I}\mathrm{d}A = -\delta G. \tag{5}$$

The integral extends over the area of the surfaces participating in diffusion. This equation defines the driving force, $\mathbf{F}$. Because (5) holds for any virtual motion, one can show that it reproduces the relation between the driving force and the curvature gradient, and the conditions of local equilibrium at a triple junction [22]. Such local relations, however, are useless to the finite element method, and will not be listed here.

Substituting (2) into (5), we obtain

$$\int \frac{\mathbf{J}\cdot\delta\mathbf{I}}{M}\mathrm{d}A = -\delta G. \tag{6}$$

The actual flux field $\mathbf{J}$ satisfies (6) for any virtual motion, as specified by a pair of fields $\delta\mathbf{I}$ and δr_n subject to (4). This is the *weak statement* of Herring's theory. The statement determines the field $\mathbf{J}$ as follows. For one virtual motion subject to (4), equation (6) gives one relation that $\mathbf{J}$ has to satisfy. Because there are infinitely many virtual motions, equation (6) gives infinitely many relations that $\mathbf{J}$ has to satisfy simultaneously. Consequently, the field $\mathbf{J}$ is solved from these relations. Once $\mathbf{J}$ is solved, the surface normal velocity is obtained from (3), which then updates the solid shape.

The statements of the surface diffusion problem differ from those of evaporation–condensation in that the former conserve solid mass, equations (3) and (4). Consequently, surface diffusion problems as formulated above are difficult to implement in a finite element setting. We next describe one approach to address the issue.

2.3. *Weak statement for combined surface diffusion and evaporation–condensation*

Imagine two concomitant processes on the surface: the solid matter can relocate on the surface by diffusion, and exchange with the surrounding vapor by evaporation–condensation. We have two reasons for looking at this combination. First the concomitant processes can occur in practice; it would be useful to have such a code. The second reason has to do with the constraint of mass conservation. As will become clear, once the weak statement includes

evaporation–condensation, the overall mass conservation is easier to treat.

To focus on the main ideas, we still assume that the free energy is the sum over all surface and grain boundary areas, equation (1). The kinetic law for evaporation–condensation is the same as that in [1]. Let p be the free energy reduction associated with per unit volume of matter added to per unit surface area of the solid, and j be the volume of matter added to per unit area of the solid surface per unit time. They are proportional to each other:

$$j = mp. \tag{7}$$

The specific evaporation–condensation rate, m, is a kinetic parameter in the model.

Mass conservation relates the surface velocity, v_n, to the fluxes of the two matter transport processes:

$$v_n = j - \nabla \cdot \mathbf{J}. \tag{8}$$

This relation replaces (3). Let δi be the volume of matter added to per unit area of the solid surface, and $\delta \mathbf{I}$ be the mass displacement as defined before. The two kinds of virtual changes together cause the surface to move in the normal direction by distance

$$\delta r_n = \delta i - \nabla \cdot (\delta \mathbf{I}). \tag{9}$$

This relation replaces (4).

Associated with the virtual motion, the free energy changes by δG. According to the definition of the two kinds of driving forces, $\mathbf{F}$ and p, matter relocation and exchange on the surface area element, δA, reduce the free energy by an amount, $(\mathbf{F}\cdot\delta\mathbf{I} + p\delta i)\mathrm{d}A$. Thus,

$$\int (\mathbf{F} \cdot \delta \mathbf{I} + p\delta i) dA = -\delta G. \tag{10}$$

The integral extends over the surface areas participating in matter transfer. The equation holds for any virtual motion subject to (9). This statement defines both $\mathbf{F}$ and p.

Substituting the kinetic laws, (2) and (7), into (10), we have

$$\int \left(\frac{\mathbf{J} \cdot \delta \mathbf{I}}{M} + \frac{j\delta i}{m} \right) dA = -\delta G. \tag{11}$$

This is a weak statement including both surface diffusion and evaporation–condensation. All three virtual quantities, $\delta \mathbf{I}$, δi and δr_n, appear in the statement. (One needs δr_n to evaluate δG.) The three virtual quantities themselves are subject to (9).

In formulating a finite element method, it is convenient to use $\delta \mathbf{I}$ and δr_n as the basic variables. Eliminating j and δi in (11) by using (8) and (9), we obtain

$$\int \left\{ \frac{\mathbf{J} \cdot \delta \mathbf{I}}{M} + \frac{(v_n + \nabla \cdot \mathbf{J})[\delta r_n + \nabla \cdot (\delta \mathbf{I})]}{m} \right\} dA = -\delta G. \tag{12}$$

In this form, the weak statement only involves two virtual fields, δr_n and $\delta \mathbf{I}$. They vary independently, subject to no constraint. The actual fields, $\mathbf{J}$ and v_n, must satisfy (12) for any small changes δr_n and $\delta \mathbf{I}$. It is this weak statement that will be used to formulate the finite element method.

The situation that matters only diffuses on the surface but does not exchange between the solid and the vapor can be treated as a limiting case by setting a small value of m. The numerical solution gives a small value of $v_n + \nabla\cdot\mathbf{J}$, namely, a negligible amount of "mass leak", and thereby conserves the solid mass approximately. One may understand the approximation as follows. Let λ be a representative length in a problem. A dimensionless ratio, $m\lambda^2/M$, measures the relative rate of evaporation–condensation and surface diffusion. When $m\lambda^2/M \ll 1$, the effect of evaporation–condensation is negligible on processes occurring at the length scale λ and any length scales smaller that λ. In the numerical simulation. We often set $m\lambda^2/M = 10^{-6}$.

3. FINITE ELEMENT METHOD

As stated above, the weak statement demands that the actual fields $\mathbf{J}$ and v_n satisfy (12) for all virtual motions. To obtain an approximate solution of $\mathbf{J}$ and v_n, one relaxes this demand. Instead of requiring that (12) be satisfied for *all* virtual motions, one requires that (12) be satisfied for *a family of* virtual motions. Obviously, the larger the family, the more accurate the approximate solution. A finite element method is one way to implement this idea.

To focus on basics, we will consider two-dimensional problems, when the solid is invariant in one direction, and its shape change can be studied in a cross-section perpendicular to that direction. In the cross-section, the solid is represented by an area, and the surface by a curve. Because the weak statement requires low order differentials only, we model the curve by an assembly of straight segments. For example, a particle is modeled by a polygon of many sides. Each segment is an element, and two neighboring elements meet at a node. The motions of the nodes constitute the family of virtual motions. In principle, the length of each element is arbitrary, and different elements can have different lengths. In practice, we place short elements where

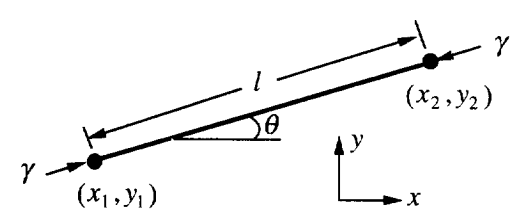

Fig. 2. A straight line element. When the element undergoes virtual motions, the free energy varies, exerting on the two nodes the axial force of magnitude γ.

a curved object is of interest, and long elements elsewhere to reduce computation time.

3.1. Interpolation on an element

Figure 2 shows one element, with two nodes at the positions (x_1, y_1) and (x_2, y_2). The element has length l and slope θ; they relate to the nodal positions by $l\sin\theta = y_2 - y_1$ and $l\cos\theta = x_2 - x_1$. Locate a point on the element by its distance from the mid-point of the element, s. When the two nodes change positions by $(\delta x_1, \delta y_1)$ and $(\delta x_2, \delta y_2)$, the element remains to be straight, elongating, translating, and rotating, according to the nodal position changes. Consequently, at point s the element moves in the normal direction by distance

$$\delta r_n = N_1\delta x_1 + N_2\delta y_1 + N_3\delta x_2 + N_4\delta y_2, \tag{13}$$

with the interpolation coefficients being

$$N_1 = -\left(\frac{1}{2} - \frac{s}{l}\right)\sin\theta,\ N_2 = +\left(\frac{1}{2} - \frac{s}{l}\right)\cos\theta$$

$$N_3 = -\left(\frac{1}{2} + \frac{s}{l}\right)\sin\theta,\ N_4 = +\left(\frac{1}{2} + \frac{s}{l}\right)\cos\theta \tag{14}$$

Similarly, when the nodes move at velocities $(\dot{x}_1, \dot{y}_1)$ and $\dot{x}_2, \dot{y}_2)$, at point s the element moves in the normal direction at velocity

$$v_n = N_1\dot{x}_1 + N_2\dot{y}_1 + N_3\dot{x}_2 + N_4\dot{y}_2. \tag{15}$$

The interpolation coefficients are the same as the above.

In two-dimensional problems, matter is restricted to diffuse along the curve in the cross-section. Consequently, the flux vector has only one component, J, and its divergence is the differentiation along the curve, $\partial J/\partial s$. Similarly, the virtual mass displacement vector has only one component, δI, and its divergence is $\partial\delta\backslash\ \mathrm{I})/\partial s$. Recall that δr_{n} and the divergence of δI appear in the same equation. Since we have interpolated δr_{n} linearly, it is natural to interpolate δI quadratically. Let δI_1, δI_2 and δI_{m} be the virtual mass displacements at the two nodes and the mid-point of the element. Interpolate the mass displacement at point s on the element by

$$\delta I = Q_1\delta I_1 + Q_2\delta I_2 + Q_m\delta I_m, \tag{16}$$

with the interpolation coefficients being

$$Q_1 = \frac{s}{l}\left(1 - \frac{2s}{l}\right),\ Q_2 = \frac{s}{l}\left(1 + \frac{2s}{l}\right),$$

$$Q_m = 1 - \left(\frac{2s}{l}\right)^2. \tag{17}$$

The same interpolation is used for the flux. Thus, if J_1, J_2 and J_m are the fluxes at the two nodes and the mid-point of the element, the flux at point s on the element is given by

$$J = Q_1J_1 + Q_2J_2 + Q_mJ_m. \tag{18}$$

In summary, each element has four degrees of freedom $(\delta x_1, \delta y_1, \delta x_2\ ), \delta y_2)$ to describe the motion of the element, and three degrees of freedom $(\delta I_1, \delta I_2, \delta I_{\mathrm{m}})$ to describe diffusion on the element. This is compared with evaporation–condensation treated in [1], where only four degrees of freedom were used.

3.2. Integration over an element

Each element has seven degrees of freedom. Write $\delta\mathbf{q}^{\mathrm{e}}$ for the column of the virtual changes in the generalized coordinates, and $\dot{\mathbf{q}}^{\mathrm{e}}$ for the column of the generalized velocities, namely,

$$\delta\mathbf{q}^e = [\delta x_1 \quad \delta y_1 \quad \delta I_1 \quad \delta x_2 \quad \delta y_2 \quad \delta I_2 \quad \delta I_m]^T$$

$$\dot{\mathbf{q}}^e = [\dot{x}_1 \quad \dot{y}_1 \quad J_1 \quad \dot{x}_2 \quad \dot{y}_2 \quad J_2 \quad J_m]^T$$

The superscript e indicates quantities for the element, and the superscript T indicates the transpose of a column.

The integral in (12) now extends over the curve representing the solid surface in the cross-section, and is evaluated element by element. For each element, the integration gives a bilinear form

$$(\delta\mathbf{q}^e)^T\,\mathbf{H}^e\dot{\mathbf{q}}^e, \tag{19}$$

with the seven by seven matrix given by

$$\mathbf{H}^e = \frac{1}{6ml}\begin{bmatrix} 2l^2S^2 & -2l^2SC & 5lS & l^2S^2 & -l^2SC & -lS & -4lS \\ -2l^2SC & 2l^2C^2 & -5lC & -l^2SC & l^2C^2 & lC & 4lC \\ 5lS & -5lC & 14+4\mu & lS & -lC & 2-\mu & -16+2\mu \\ l^2S^2 & -l^2SC & lS & 2l^2S^2 & -2l^2SC & -5lS & 4lS \\ -l^2SC & l^2C^2 & -lC & -2l^2SC & 2l^2C^2 & 5lC & -4lC \\ -lS & lC & 2-\mu & -5lC & 5lC & 14+4\mu & -16+2\mu \\ -4lS & 4lC & -16+2\mu & 4lS & -4lC & -16+2\mu & 32+16\mu \end{bmatrix} \tag{20}$$

where we have used the shorthand notation $\mu = (ml^2)/(5\,M)$, $S = \sin\theta$ and $C = \cos\theta$. This matrix may be compared with the four by four matrix used for evaporation–condensation in [1].

3.3. Forces on nodes by an element

For two-dimensional problems, we use the free energy per unit length, and (1) becomes a sum over

all element lengths, $G=\sum \gamma l$. When the two nodes of an element change positions by $(\delta x_1, \delta y_1)$ and $(\delta x_2, \delta y_2)$, the element length changes by

$$\delta l = -\cos\theta\delta x_1 - \sin\theta\delta y_1 + \cos\theta\delta x_2 + \sin\theta\delta y_2.$$

This causes the free energy to change by

$$\gamma\delta l = -f_1\delta x_1 - f_2\delta y_1 - f_3\delta x_2 - f_3\delta y_2 \qquad (21)$$

with

$$f_1 = \gamma\cos\theta, f_2 = \gamma\sin\theta,$$
$$f_3 = -\gamma\cos\theta, f_4 = -\gamma\sin\theta. \qquad (22)$$

They are forces acting on the two nodes (see Fig. 2). The surface tension tends to cause the element length to shrink. Because the free energy depends on the solid shape, there are no forces associated with the nodal mass displacements.

3.4. Global viscosity matrix and force column

The rest of the procedure follows that of a standard finite element method [16], and is briefly outlined here. Model a surface with k elements and n nodes. For each element, the mid-point has one degree of freedom, the flux. Each node has three degrees of freedom, the two velocities and the flux. The model has $k + 3n$ degrees of freedom in total. Assemble all the nodal velocities and the nodal fluxes into a column $\dot{\mathbf{q}}$, and all the virtual nodal movements and mass displacements into a column δb q. Summing over all the elements, (12) becomes

$$\delta\mathbf{q}^T\mathbf{H}\dot{\mathbf{q}} = \delta\mathbf{q}^T\mathbf{f}. \qquad (23)$$

The matrix $\mathbf{H}$ and the column $\mathbf{f}$ are assembled from the contributions of all the elements.

We require that the approximate solution, $\dot{\mathbf{q}}$, satisfy (12) for all virtual motions in the family. Consequently, equation (23) holds for any $\delta\mathbf{q}$, so that

$$\mathbf{H}\dot{\mathbf{q}} = \mathbf{f}. \qquad (24)$$

We call $\mathbf{H}$ the viscosity matrix. Equation (24) is a set of linear algebraic equation for the generalized velocities. Once solved, the nodal velocities update the nodal positions for a small time step. The procedure repeats for many time steps to simulate large shape change. Static condensation [16] can be used to eliminate the fluxes at the mid-point of all elements from the list of the generalized coordinates. Other numerical considerations in [1] apply. In the following two sections, we illustrate the use of the finite element program with examples.

4. THERMAL GROOVING

On a polycrystal surface, a triple junction appears when a grain boundary meets the surface. When heated, matter diffuses on the surface, causing the surface to groove, leaving depression along the triple junctions and bumps over the grains. The size of each groove increases with the time. Mullins [4] analyzed the growing groove by solving a differential equation. He considered an earlier stage, when the groove size is much smaller than the grain size, and each pit, formed on the surface where a three-grain junction meets the surface, is also small. Consequently, the grooves over adjacent grain boundaries grow independently, and he could study a single groove in a cross-section perpendicular to the triple junction, as in Fig. 3. If the groove size is sufficiently small, the effect of evaporation–condensation is negligible. Because surface diffusion conserves solid mass, two bumps grow on the grains at the expense of the mass leaving the groove.

The triple junction is pulled down by the grain boundary tension, γ_b. Let M be the surface diffusion mobility, and γ_s the surface tension. Mullins assumed that the polycrystal surface is flat at the initial time. This initial configuration, Fig. 3(a), has no length scale. The dynamics of the problem, however, does have a length scale, $(M\gamma_s t)^{1/4}$, which increases with the time t. Consequently, the groove profiles are self-similar at all times. The size of the groove scales with the length $(M\gamma_s t)^{1/4}$. Mullins further assumed that the ratio γ_b/γ_s is sufficiently small, so that the surface slope is small everywhere, and the differential equation can be linearized. Figure 4 plots the surface profile obtained by Mullins for several values of γ_b/γ_s.

As shown in the Appendix, the non-linear differential equation can also be solved numerically without being linearized. This non-linear solution is included in Fig. 4. Evidently, Mullins's linear solution is an excellent approximation for small values of γ_b/γ_s. The difference between the linear and the non-linear solutions can be seen only when γ_b/γ_s is large.

We used this example to check the accuracy of the finite element program. The surface of one

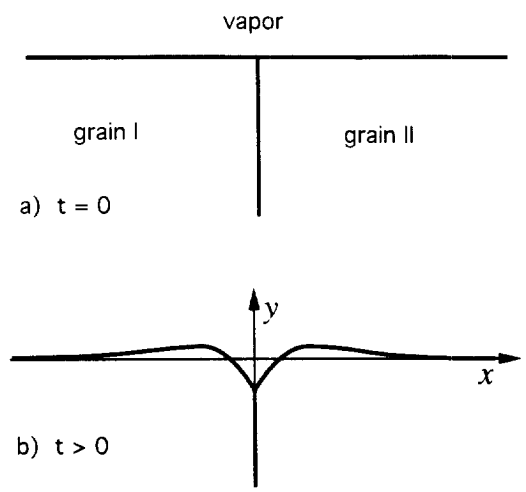

Fig. 3. A triple junction of a grain-boundary and a surface. (a) At $t = 0$, the surface is flat, (b) at a finite time, the surface grooves as matter diffuses on the surface.

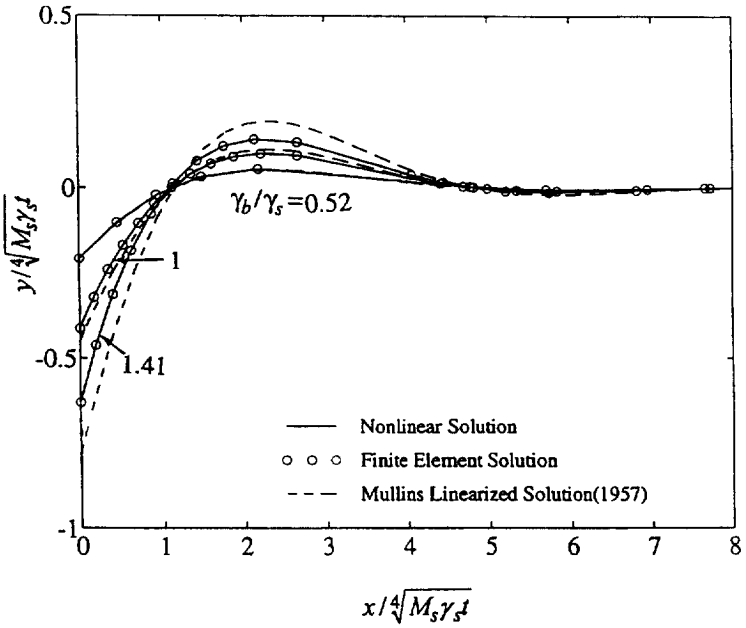

Fig. 4. A comparison of groove profiles solved by three methods.

grain was modeled with about 40 elements. The effect of the grain boundary was represented by a force of magnitude γ_b, acting on the triple junction, in the direction along the grain boundary. In a very short time, the dihedral angle at the triple junctions reached the equilibrium value. As explained in Part I [1], this is characteristic of the finite element method: the equilibrium dihedral angle need not be prescribed, but comes out as a part of the solution. The smaller the elements, the shorter the time needed to approach the equilibrium dihedral angle. In the simulation, the surface shape quickly became self-similar, with the groove depth scaling with $(M\gamma_s t)^{1/4}$. The finite element solutions agree with the non-linear solutions (Fig. 4).

5. COMPETITIVE GRAIN BOUNDARY MOTION AND SURFACE GROOVING

A polycrystalline thin film, as deposited on a single crystal substrate at a relatively low temperature, typically has small grains, no larger than the film thickness. Upon annealing, the in-plane grain diameter can sometimes grow substantially larger than the film thickness. Thompson and co-workers have studied this phenomenon with many materials combinations. One mechanism relates to surface tension anisotropy [24]. Consider two neighboring grains, both through the film thickness. Because the crystalline orientations differ, the two grains have different surface tensions. To reduce the total free energy, the grain with the smaller surface tension may grow at the expense of the other grain. Similarly, the film–substrate interface may have different tensions for the two grains. The growing grain should have the lower combined free energy.

It is also commonly observed that, upon annealing, the film surface may groove along triple junctions, and break the film into islands [e.g. 25]. Evidently, an energetic consideration by itself is inadequate to select the morphology. The system selects morphology *dynamically*, according to the relative rate of the two competitive motions. If the grain boundaries move faster, the film remains continuous and forms large grains. If the surface grooves faster, the film breaks into islands.

We will illustrate the competitive motions with an ideal situation shown in Fig. 5. The annealing has reached a late stage, when the grain size in the plane of the film is much larger than the film thickness. We examine whether the grain boundary will still move laterally, or whether the film surface will groove down to break the film. So idealized, the problem becomes two-dimensional, with the cross-sectional view in Fig. 5. The grain-boundary tension is γ_b, and the grain boundary mobility is m_b (as defined in [1]). For simplicity, the two grains, labeled as + and −, are assumed to have identical surface tension γ_s, and identical surface diffusion mobility M_s. The film–substrate interface, however,

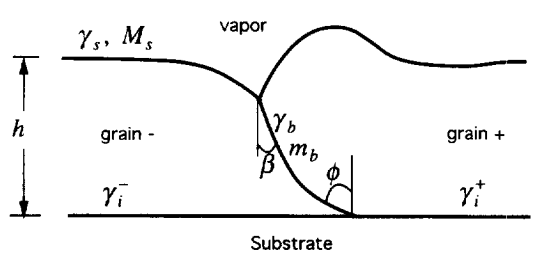

Fig. 5. A grain-boundary migrates in a thin film, driven by the difference in the interface tensions.

has different tensions for the two grains, γ_i^+ and γ_i^-. It is this difference that motivates grain $-$ to grow at the expense of grain $+$. Far away from the triple junction, the film thickness is h.

At the junction where the grain boundary meets the film–substrate interface, the various tensions balance in the horizontal direction, giving the grain-boundary angle at the junxtion, ϕ, by

$$\sin\phi = \frac{\gamma_i^+ - \gamma_i^-}{\gamma_b}. \tag{25}$$

The larger the interface tension difference, the larger the angle ϕ. We will call ϕ the pulling angle for the grain boundary motion.

After a sufficiently long time, the motion may reach a steady state. That is, the grain boundary and the triple junction move together to the right, at a constant velocity, with invariant shapes. In particular, the groove depth remains constant during the motion. Mullins analyzed a steadily translating triple junction [5], and found that the grain boundary makes an angle at the triple junction, given by

$$\beta = \frac{\gamma_b}{6\gamma_s}. \tag{26}$$

The total volume of the two grains is conserved: a bump forms on the parent grain, and a depression on the growing grain.

In his original paper [5], Mullins did not specify a cause for the grain boundary motion, and left the steady state velocity undetermined. In the present model, the cause for motion is the difference in the interface tensions. To move steadily to the right, the grain boundary must be concave to the right—that is, the angles at the two triple junctions must satisfy

$$\phi > \beta. \tag{27}$$

This places a condition on various tensions, namely,

$$\frac{\gamma_i^+ - \gamma_i^-}{\gamma_b} > \frac{\gamma_b}{6\gamma_s}. \tag{28}$$

In particular, because $\beta \neq 0$, a small difference in the interfacial tensions may be insufficient to pull the grain boundary steadily. For all cases discussed below, we set $\gamma_s = \gamma_b$, so that $\beta = 9.5°$. A steady state requires a pulling angle $\phi > 9.5°$.

In a previous paper [26], we obtained an analytic solution to the combined steady motion of the grain boundary and the triple junction. Here we will examine the transient motion using the finite element program. We combine the program for the surface diffusion developed in this paper and that for the grain boundary migration developed in [1]. Starting with an initial geometry, the combined program simulates the evolving shape. Even for this idealized problem, there are many variables. We can vary the initial geometry, vary energetics by the pulling angle ϕ, and vary kinetics by the dimensionless ratio $M_s/(h^2 m_b)$. In the simulation, ϕ is controlled by prescribing the interface tensions, corresponding to a horizontal force acting on the triple junction on the interface. The time is given in the unit of $h^2/(m_b \gamma_b)$.

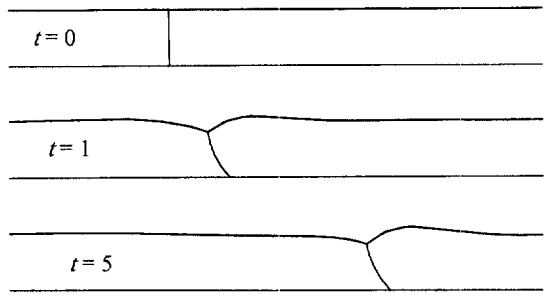

Fig. 6. The film surface is initially flat, $M_s/(h^2 m_b) = 10^{-1}$ and $\phi = 45°$.

Figure 6 shows a transient sequence for a system with $M_s(h^2 m_b) = 10^{-1}$ and $\phi = 45°$. At $t = 0$, the initial geometry consists of a flat film surface and a vertical grain-boundary. The pulling angle is so large that, at $t = 1$, the steady state has already emerged. At $t = 5$, the grain boundary has traveled for some distance from its initial position. Both the steady groove depth and the steady velocity agree with the analytic solution in [26].

Figure 7 shows another sequence for a system with the same kinetic and energetic parameters, but a different initial geometry: a notch of depth $0.2\,h$ and angle 120° is introduced at the triple junction. The triple junction moves up, and quickly reaches the steady state. This example shows that, when the pulling angle ϕ is large, the steady state is very robust, overcoming unfavorable initial conditions.

Figure 8 shows the sequence for a lower surface mobility. Because of the large pulling angle, the grain boundary quickly breaks away from the notch, and moves steadily under a shallow groove. A dent is left behind the triple junction, corresponding to a "ghost boundary" sometimes observed in experiments. After the breakaway, the grain-boundary moves rapidly, but the dent heals slowly.

Comparing Figs 7 and 8, we can appreciate the effect of the kinetic parameter, $(M_s/(h^2 m_b)$. For the

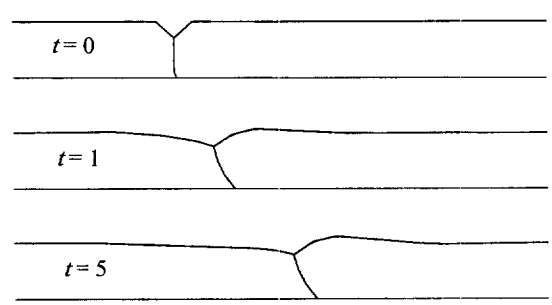

Fig. 7. The film surface has an initial notch, $M_s/(h^2 m_b) = 10^{-1}$ and $\phi = 45°$.

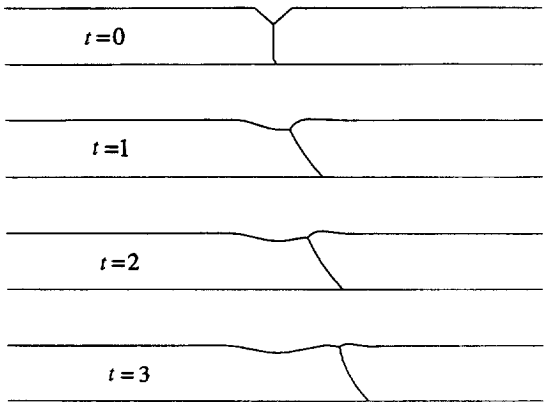

Fig. 8. The film surface has an initial notch, $M_s/(h^2 m_b) = 10^{-3}$ and $\phi = 45°$.

same energetics, the steady groove depth increases with this kinetic parameter. Consequently, even when a system has the energetics favoring grain boundary motion, a large value of $M_s/(h^2 m_b)$ may cause the film to break. This condition corresponds to a large surface diffusivity, a small grain boundary mobility, or a small film thickness. These quantities may be controlled experimentally to select one film morphology or the other. A morphological selection map, calculated from the steady state solution, was presented in [26].

Figure 9 shows a transient sequence for a system with a small angle, $\phi = 5°$, which cannot pull the grain boundary into steady motion. The initial geometry consists of a flat surface and a vertical grain-boundary. The grain-boundary is pinned by triple junction at the film surface, and pulled by the triple junction at the film–substrate interface. The surface grooves down, breaking the film eventually. Note that the grain-boundary is nearly straight at all times, suggesting a very small driving force on the grain-boundary. When the pulling angle is small, even for a relatively small surface diffusivity, $M_s/(h^2 m_b) = 10^{-2}$, the surface groove can effectively pin the grain-boundary.

6. CONCLUDING REMARKS

We have formulated a weak statement for combined surface diffusion and evaporation–condensation. The statement is applicable for tracing arbitrarily large shape change in two or three dimensions. On the basis of the statement, a finite element program is developed for two dimensional problems. The program is combined with that for grain-boundary motion to simulate evolving structure in a polycrystal. Numerical examples demonstrate that the method is accurate and robust, and can capture intricate details. The method may not be the fastest for any particular problems, but is applicable to many problems, and can readily include multiple energetic forces and rate processes.

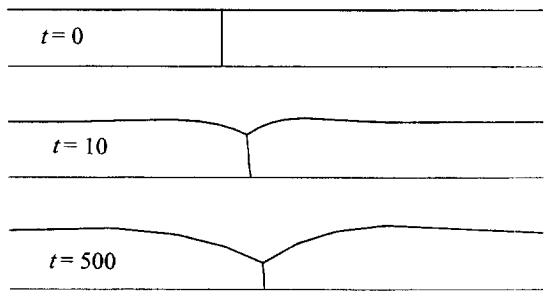

Fig. 9. The difference in interface tension is too small to pull the grain boundary into steady motion, $M_s/(h^2 m_b) = 10^{-2}$ and $\phi = 5°$.

Consequently, it is a promising candidate for a general-purpose simulation tool.

Acknowledgements—The work was supported by NSF through grant MSS-9258115, and by an Alcoa Foundation grant. Discussion with Professor W. Yang at the early stage of the work was helpful.

REFERENCES

1. Sun, B., Suo, Z. and Yang, W., *Acta mater.*, 1997, **45**, 1907.
2. Herring, C., in *The Physics of Powder Metallurgy*, ed. W. E. Kingston. McGraw-Hill, New York, 1951, p. 143.
3. Prigogine, I., *Introduction to Thermodynamics of Irreversible Processes*. Wiley, New York, 1967.
4. Mullins, W. W., *J. Appl. Phys.*, 1957, **28**, 333.
5. Mullins, W. W., *J. Acta metall.*, 1958, **6**, 414.
6. Mullins, W. W., *J. Appl. Phys.*, 1959, **30**, 77.
7. Asaro, R. J. and Tiller, W. A., *Metall. Trans.*, 1972, **3**, 1789.
8. Chiu, C. H. and Gao, H., *Int. J. Solids Structures*, 1993, **30**, 2981.
9. Spencer, B. J., Voorhees, P. W. and Davis, S. H., *Phys. Rev. Lett*, 1991, **67**, 3696.
10. Chuang, T-J. and Rice, J. R., *Acta metall.*, 1973, **21**, 1625.
11. Thouless, M. D., *Acta metall.*, 1993, **41**, 1057.
12. Pharr, G. M. and Nix, W. D., *Acta metall.*, 1979, **27**, 1615.
13. Hsueh, C. H., Evans, A. G. and Coble, R. L., *Acta metall.*, 1982, **30**, 1268.
14. Yang, W. H. and Srolovitz, D. J., *Phys. Rev. Lett.*, 1993, **71**, 1593.
15. Kraft, O. and Arzt, E., *Acta mater.* 1997.
16. Zienkiewicz, O. C. and Taylor, R. L., *The Finite Element Method*. McGraw Hill, New York, 1994.
17. Needleman, A. and Rice, J. R., *Acta metall.*, 1980, **28**, 1315.
18. Cocks, A. C. F., *Acta metall. mater.*, 1994, **42**, 2197.
19. Sofronis, P. and McMeeking, R. M., *Mech. Mater.*, 1994, **18**, 55.
20. Suo, Z. and Wang, W., *J. Appl. Phys.*, 1994, **76**, 3410.
21. Svoboda, J. and Riedel, H., *Acta metall. mater.*, 1995, **43**, 1.
22. Suo, Z., *Advances in Applied Mechanics*, 1997, **33**, 194.
23. Carter, W. C., Roosen, A. R., Cahn, J. W. and Taylor, J. E., *Acta metall. mater.*, 1995, **43**, 4309.
24. Thompson, C. V., Floro, J. and Smith, H. I., *J. Appl. Phys.*, 1990, **67**, 4099.

25. Miller, K. T. and Lange, F. F., *J. Mater. Res.*, 1991, **6**, 2387.
26. Sun, B., Suo, Z. and Yang, W., Mat. Res. Soc. Symp. Proc. in press.

APPENDIX

Non-linear equations for self-similar grooving profile

With reference to Fig. 3, let the x-axis coincide with the initial surface, and the y-axis with the grain boundary. Identify a point on the surface by its coordinates (x, y), and the surface profile at the time t by a function, $y(x,t)$. Let s be the curve length measured along the surface from the triple junction to a point on the surface, and θ be the angle from the x-axis to the surface tangent, and K be the curvature; they are all functions of x and t. At a fixed time, the following relations of differential geometry apply:

$$\frac{\partial x}{\partial s} = \cos\theta, \frac{\partial y}{\partial s} = \sin\theta, K = -\frac{\partial \theta}{\partial s}. \tag{A1}$$

Following Refs [2 and 4], we assume that the flux is proportional to the curvature gradient, namely,

$$J = -M\gamma_s \frac{\partial K}{\partial s}. \tag{A2}$$

Mass conservation requires that

$$\frac{\partial y(x,t)}{\partial t} = -\frac{\partial J(x,t)}{\partial x}. \tag{A3}$$

The partial differential equations need to be solved subject to the following initial and boundary conditions. The initial surface is flat:

$$y(x,0) = 0. \tag{A4}$$

Remote from the triple junction, the surface is flat at all time:

$$y(\infty, t) = 0. \tag{A5}$$

At the triple junction, the surface slope is fixed in all time by the local equilibrium condition:

$$\sin\theta = \frac{\gamma_b}{2\gamma_s}, \text{at triple junction.} \tag{A6}$$

The flux vanishes at the triple junction:

$$J = 0, \quad \text{at triple junction.} \tag{A7}$$

Normalize all the lengths, x, y, s and $1/K$, by $(M\gamma_s t)^{1/4}$, and normalize J by $(M\gamma_s t)^{1/2}$. The geometric relations in (A1) keep the same forms. Equation (A2) becomes

$$J = -\frac{\partial K}{\partial s}. \tag{A8}$$

Here we have used the same notation for the normalized quantities J, K and s. Denote $X = (M\gamma_s t)^{1/4}x$ and $Y = (M\gamma_s t)^{1/4}y$. The self-similar profile is described by a function of one variable, $Y(X)$. Equation (A3) becomes

$$\frac{1}{4}\left(Y - X\frac{dY}{dX}\right) = -\frac{dJ}{dX}. \tag{A9}$$

In terms of the normalized quantities, the above partial differential equations reduce to a set of ordinary differential equations:

$$\begin{aligned} \frac{dY}{dX} &= \tan\theta \\ \frac{d\theta}{dX} &= -\frac{K}{\cos\theta} \\ \frac{dK}{dX} &= -\frac{J}{\cos\theta} \\ \frac{dJ}{dX} &= -\frac{1}{4}(Y - X\tan\theta) \end{aligned} \tag{A10}$$

These non-linear equations govern the functions $Y(X)$, $\theta(X)$, $K(X)$, $J(X)$.

In terms of the normalized quantities, both (A4) and (A5) reduce to the same boundary condition remote from the triple junction, i.e. $Y(\infty) = 0$. Physically it is evident that θ, K, J should all vanish at $X = \infty$. The boundary conditions at the triple junction, (A6) and (A7), set the slope and flux at $X = 0$. The normalized problem has only one parameter, γ_b/γ_s, which enters through the boundary condition (A6).

The boundary value problem is solved numerically by a shooting method. We use the triple junction, $X = 0$, as the initial point. Prescribed at this point are the slope $\theta(0)$ and the flux $J(0)$. We guess values for $Y(0)$ and $K(0)$, and then integrate the ordinary differential equations (A10) using a Runge–Kutta method to a large value of X. The goal is to guess such values of $Y(0)$ and $K(0)$ that everything vanishes at $X = \infty$. This is a non-linear algebraic problem for $Y(0)$ and $K(0)$. The surface profiles so determined are included in Fig. 4.